CHEMISTRY OF MATERIALS

Article

pubs.acs.org/cm

Coexisting Ferromagnetic and Ferroelectric Order in a $CuCl_4$-based Organic–Inorganic Hybrid

Alexey O. Polyakov, Anne H. Arkenbout, Jacob Baas, Graeme R. Blake, Auke Meetsma, Antonio Caretta, Paul H. M. van Loosdrecht, and Thomas T. M. Palstra*

Zernike Institute for Advanced Materials, University of Groningen, Nijenborgh 4, 9747AG Groningen, The Netherlands

Supporting Information

ABSTRACT: We investigate the structural, magnetic, and dielectric properties of the organic–inorganic hybrid material $CuCl_4(C_6H_5CH_2CH_2NH_3)_2$ and demonstrate that spontaneous ferroelectric order sets in below 340 K, which coexists with ferromagnetic ordering below 13 K. We use X-ray diffraction to show that the electric polarization results from the spatial ordering of hydrogen bonds that link the organic block comprised of phenylethylammonium cations to the inorganic copper chloride block. The hydrogen bond ordering is driven by buckling of the corner-linked copper chloride octahedra. Because the magnetic exchange pathways are also determined by this octahedral buckling, a potentially large magnetoelectric coupling is induced. Our results imply that such hybrids form a new family of multiferroic materials.

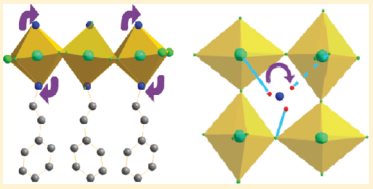

KEYWORDS: *multiferroic, ferroelectric, ferromagnetic, organic–inorganic hybrid, metal-oxide framework*

INTRODUCTION

The coexistence of ferromagnetic and ferroelectric order in a single material requires sophisticated materials design. Ferroelectricity is associated in most materials with atoms that have empty d-orbitals, whereas magnetism requires partially filled d-orbitals. During recent years, there has been enormous interest in the field of multiferroics,[1,2] after it was shown that ferroelectricity can be introduced by alternative routes such as magnetic cycloidal order,[3] charge ordering,[4] and spin-Peierls distortion.[5]

Not only is the combination of ferroelectricity and ferromagnetism of importance for potential applications, but the strength of the coupling between these order parameters must also be considered.[6−8] This coupling can allow the direct control of the magnetization by an electric field and vice versa. This facilitates more efficient data storage architectures and can also be used in spin-polarized devices for spintronics.

Perovskite-based organic–inorganic hybrid compounds[9] are excellent candidates to show multiferroic order, because they combine structural flexibility with robust magnetic and electrical properties: 1. the inorganic backbone of these hybrids is formed by strongly connected metal–halogen octahedra, which allow robust magnetic interactions; 2. the arrangement of hydrogen bonds between the halogen atoms and the ammonia end group of the organic component resembles the hydrogen-bond network of ferroelectrics[10] such as ammonium Rochelle salt (ARS)[11] and triglycinesulfate (TGS).[12] The potential of hybrid organic–inorganic compounds as a new route toward multiferroics has been emphasized by Jain et al.[13] and Ramesh.[14]

Here, we investigate the structural, dielectric, and magnetic properties of $CuCl_4(C_6H_5CH_2CH_2NH_3)_2$ and demonstrate that it exhibits improper ferroelectric order below 340 K that coexists with ferromagnetic order below 13 K. We propose a structural mechanism based on hydrogen bond ordering for the breaking of inversion symmetry. This mechanism may be general for hybrid materials in which the inorganic and organic blocks are linked by hydrogen bonds.

EXPERIMENTAL SECTION

Synthesis. We synthesized the organic–inorganic hybrid $CuCl_4(C_6H_5CH_2CH_2NH_3)_2$, previously reported by Arkenbout et al.,[15] through self-assembly crystallization from an aqueous solution of 2-phenylethylammonium chloride and $CuCl_2{\cdot}2H_2O$ salts, by slowly evaporating water at room temperature. Crystals in the form of square brown plates with dimensions of a few mm were obtained.

Single Crystal X-ray Diffraction. Single crystal X-ray diffraction was performed using a three-circle Bruker Apex diffractometer equipped with a CCD detector and operating with Mo Kα radiation. Data were collected at 100 K and 370 K and processed using the SMART software.[16] The structure was solved by Patterson methods, and the extension of the model was accomplished by direct methods applied to difference structure factors using the program DIRDIF[17] and then refined using SHELX97.[18] The hydrogen atoms were generated by geometrical considerations and constrained to their idealized positions. The amine group was refined as a rigid body that was allowed to rotate freely.

Magnetic Measurements. A Quantum Design XL MPMS SQUID magnetometer was used to carry out magnetic measurements. The crystal was placed in a gelatin capsule and fixed in place with cotton.

Calorimetry Measurements. Above room temperature, simultaneous differential scanning calorimetry (DSC) and thermogravimetric analysis (TGA) measurements were performed using a TA-Instruments STD 2960; in the 210 to 360 K domain, a TA-Instruments DSC 2920 was used with a heating rate of 5 K per minute.

Received: August 10, 2011
Revised: November 30, 2011
Published: December 7, 2011

Electrical Measurements. Pyroelectric current and capacitance measurements were performed using an INSTEC probe station with SuS MicroTech probes, a Keithley 6517A multimeter, and an Andeen Hagerling 2500A ultraprecision capacitance bridge. Silver paint was used to make contacts. Birefringence measurements were performed using a Leica MZ6 microscope with a built-in polarized light source and a polarized lens.

Raman Spectroscopy. Raman spectroscopy was performed in the backscattering configuration using a triple grating micro-Raman spectrometer (T64000-Jobin Yvon). The resolution of the spectrometer was better than 2 cm^{-1} and the krypton 647 nm line was used as the excitation frequency. The sample was mounted inside an optical flow cryostat, which allows temperature control to within 0.1 K.

RESULTS

Single crystal X-ray diffraction measurements revealed a two-dimensional layered structure consisting of $CuCl_4$ inorganic sheets formed by corner-sharing copper chloride octahedra; successive inorganic sheets are interleaved by two layers of phenylethylammonium molecules (Figure 1). At 100 K, the

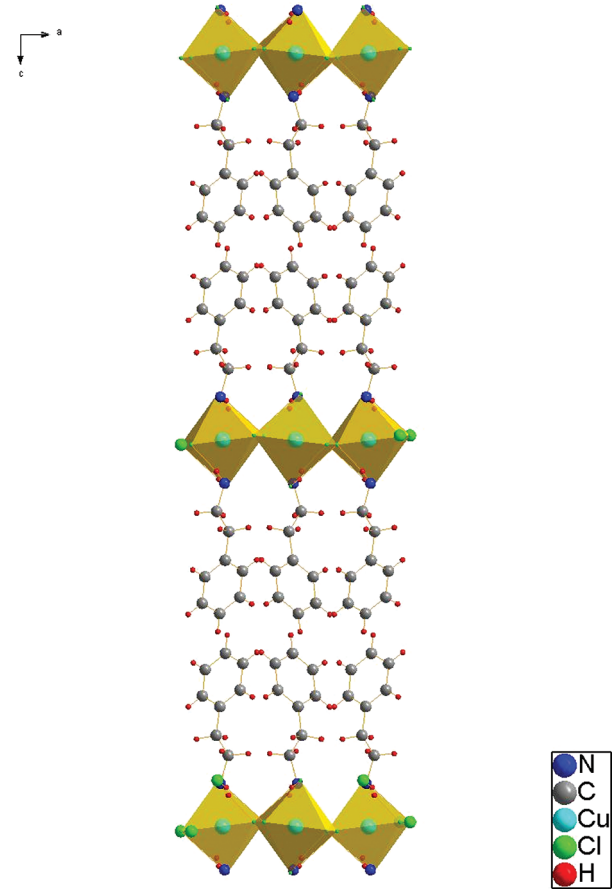

Figure 1. Crystal structure of $CuCl_4(C_6H_5CH_2CH_2NH_3)_2$ determined by single crystal X-ray diffraction at 100 K.

data were consistent with the *Pbca* space group with unit cell parameters a = 7.2099, b = 7.2664, c = 38.238 Å. The resulting structural refinement using 2340 reflections provided the bond distances and angles summarized in Table 1 ($R(F)$ = 0.0400). Our structure is consistent with that previously reported by Willett et al.[19] A CIF file is included in the Supporting Information. The distance between two adjacent inorganic planes is approximately 2 nm. Neighboring phenyl rings in the organic layers are perpendicular to each other; thus there is no

Table 1. Selected Structural Parameters of $CuCl_4(C_6H_5CH_2CH_2NH_3)_2$ Obtained by Single-Crystal X-ray Diffraction Below and Above T_c = 340 K[a]

	$T < T_c$ (100 K)	$T > T_c$ (370 K)
space group	*Pbca*	*Cmca*
Z	4	4
$R(F)$	0.0400	0.0544
GooF	1.329	1.119
a	7.2099(9)	39.021(8)
b	7.2664(9)	7.3430(15)
c	38.238(5)	7.3939(15)
V	2003.3(4)	2118.6(7)
M−M distance	5.188	5.210
M−Cl distance ⊥ c	2.8531(9), 2.2879(9)	2.9192(13), 2.2912(13)
M−Cl distance // c	2.3036(8)	2.2890(16)
M−Cl−M angle	169.15(3)	179.48(5)
Cl−M−Cl angles	88.17(3), 89.72(3), 89.64 (3)	90.0(−),90.0(−), 89.67(4)
Cl−M−c-axis angle	6.63	0

[a]Distances are expressed in Ångstroms, and angles are expressed in degrees.

significant $\pi-\pi$ overlap. Due to the Jahn−Teller effect, which is common in Cu^{2+}-based complexes, the octahedra in the inorganic sheet are distorted. The Cu−Cl bonding pattern is analogous to that found in the alkane-based Cu-hybrids.[20−22] The long axis of a given octahedron lies in the inorganic plane and is oriented along the crystallographic a- or b-axis, perpendicular to the long axis of the neighboring octahedra in order to obtain an antisymmetric wave function. This alternation of long and short bonds results in long-range orbital order. The magnetic spin is located in the $d_{x^2-y^2}$ orbital, which aligns with the long axis of the octahedron. Thus, the orbitals on neighboring metal ions are orthogonal to each other, and the spins experience ferromagnetic superexchange via a 180° Cu−Cl−Cu pathway.[23] This leads to long-range ferromagnetic order below 13 K, as shown by the temperature dependence of the magnetic susceptibility in Figure 2a and in reasonable

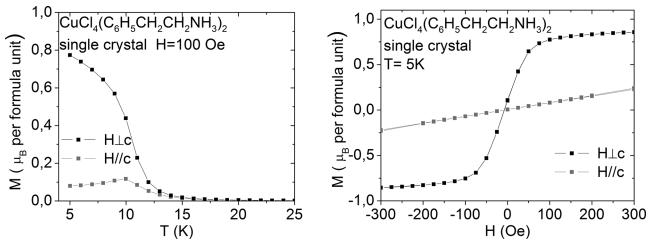

Figure 2. Magnetic susceptibility versus temperature (left) measured in a field of 100 Oe applied parallel and perpendicular to the c-axis, showing ferromagnetic ordering below 13 K. Magnetization versus applied magnetic field at 5 K (right).

agreement with the previous study of Estes et al.[24] The magnetic behavior of the related $(C_2H_5NH_3)_2CuCl_4$ hybrid, studied by de Jongh et al.[25] was consistent with ferromagnetic layers, coupled by weak antiferromagnetic interaction. The magnetization versus magnetic field for the Cu-hybrid at 5 K is shown in Figure 2b. The magnetization nearly saturates at a value of 0.8 μ_B/f.u. in a field of only 100 Oe; this corresponds to 80% of the theoretical value. This behavior agrees with previous studies of this hybrid.[24] The high temperature phase transitions were analyzed by heat flow measurements using

dx.doi.org/10.1021/cm2023696 | Chem. Mater. 2012, 24, 133−139

differential scanning calorimetry. Figure 3 (inset) shows the heat flow above room temperature. The Cu-hybrid material

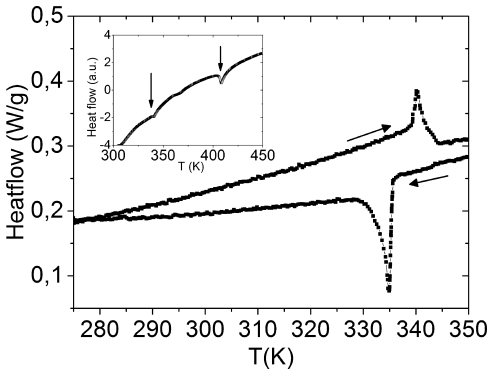

Figure 3. Differential scanning calorimetry measurements performed in two temperature regimes.

decomposes at 460 K. Between room temperature and decomposition, two phase transitions appear at 340 and 410 K. Both transitions show a peak in the heat flow caused by latent heat or a delta function in the specific heat, characteristic of first-order phase transitions. A detailed inspection of the heating and cooling curves near the phase transition at 340 K (Figure 3) provides evidence for hysteresis, also characteristic of a first-order phase transition. At a lower heating rate of 1 K/min the same hysteresis was observed and thus does not originate from a delay in temperature. Although the transition is first-order, it is accompanied by fluctuations, as can be seen by the different slopes below and above the transition and the difference in curvature below the peak in the heating and cooling curves. Therefore, it is appropriate to describe this transition as weakly first-order, similar to that observed in ammonium halides[26] and liquid crystals.[27]

In an earlier study,[11] it was proposed that organic–inorganic hybrid materials can exhibit electric polarization in the case of particular rearrangements of the hydrogen bonds.[10] The most convincing technique to confirm this behavior is the measurement of pyroelectric current. When heating a poled sample through the T_c, the disappearance of polarization generates an electric current, resulting from charge displacements. The pyroelectric current measurement performed on our Cu-hybrid is shown in Figure 4 (inset). Poling of the sample was

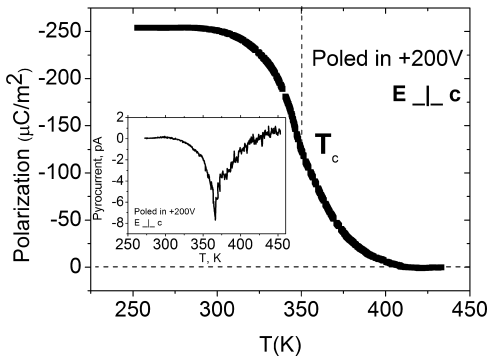

Figure 4. Temperature dependence of the pyroelectric current (inset) and the polarization perpendicular to the *c*-axis.

performed by cooling in an applied electric field of +200 V perpendicular to the *c*-axis. After removing the electric field, the current was measured while heating the sample through T_c. At the phase transition, the polarization disappears and a current is generated to compensate the charge displacement. When the sign of the poling electric field is reversed, it results in a current in the opposite direction. The polarization as a function of temperature was obtained by integrating the pyroelectric current with respect to time. Figure 4 displays the disappearance of the polarization above T_c. The magnitude of the measured polarization is approximately 250 $\mu C/m^2$ perpendicular to the *c*-axis.

The pyroelectric current measurements prove that the Cu-hybrid is polar below 340 K. Evidence for polar order below 340 K can also be observed in measurements of the capacitance versus temperature, which display a sharp jump at the transition temperature, as shown in Figure 5. However, these measurements do not allow a distinction to be made between pyroelectric and ferroelectric materials.

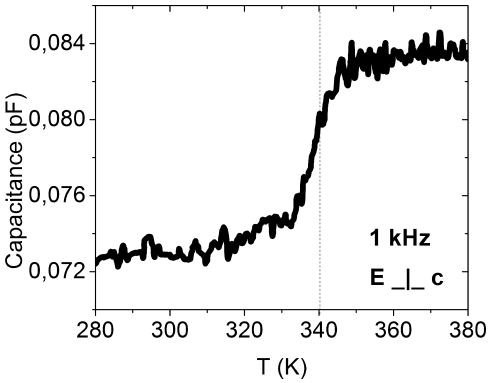

Figure 5. Temperature dependence of the capacitance measured perpendicular to the *c*-axis in the vicinity of 340 K at a frequency of 1000 Hz. The capacitance shows a sharp step at the phase transition.

Raman spectroscopic analysis of the low frequency librational modes of the organic cation confirms the weakly first-order character of the transition. As shown in Figure 6, the intensity

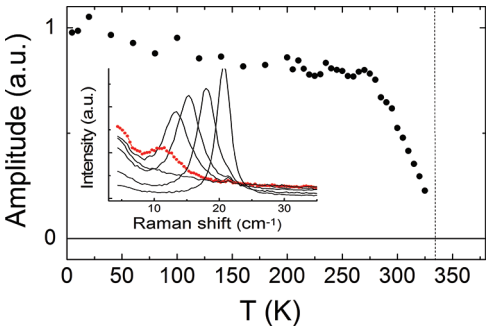

Figure 6. Amplitude of a Raman-active A_g organic libration mode at ~15 cm^{-1} as a function of temperature. The inset shows low-frequency Raman spectra above and below T_c. The decrease in amplitude, energy softening, and broadening of this mode on warming through T_c are typical effects of translational symmetry breaking.

of a Raman active A_g mode at ~15 cm^{-1} (room temperature) decreases above 270 K and becomes essentially zero at 340 K. This observation can be explained by an orientational melting of the organic molecules. The intensity of the mode is related to the order parameter that describes the translational symmetry breaking.[28] The observed broadening and softening

dx.doi.org/10.1021/cm2023696 | *Chem. Mater.* 2012, 24, 133–139

of the mode and the increase in quasi-elastic scattering on warming are characteristic features of such order−disorder-type phase transitions.[29] The pronounced temperature dependence of the intensity between ~270 K and T_c is due to the presence of fluctuations, which clearly demonstrates the weak character of the phase transition. The weakly first-order nature of the transition suggests that the material is an improper ferroelectric. In this case, the polarization is not the primary order parameter of the phase transition but is instead a side-effect of a transition that is initiated by the primary order parameter. As a result, the capacitance shows a step-like feature instead of the divergence of the dielectric constant that is common for proper ferroelectrics. We note that the classic example of a hydrogen-bond-type improper ferroelectric, ARS,[11,30] shows a ferroelectric transition at 110 K with a polarization of 2200 μC/m^2, about 10 times larger than the polarization that we measure in the Cu-hybrid.

The proof of ferroelectricity would be to measure a ferroelectric hysteresis loop, in which the pyroelectric current is measured under a cycled applied electric field. Above the coercive field the polarization reverses, which results in a peak in the pyroelectric current. The integration of such pyroelectric current curves for both negative and positive electric field sweeps would then result in a ferroelectric hysteresis loop. Thus far, attempts to measure ferroelectric loops on our hybrid material have not been successful: the polarization is 3 orders of magnitude lower than in well-known ferroelectrics such as $BaTiO_3$.[31] Therefore, such a loop would be difficult to resolve even if the Cu-hybrid is ferroelectric. At high voltages, leakage currents dominate the measurements and any small current due to a polarization reversal remained undetected.

Another method that we used to visualize the appearance of the polar phase below T_c was to monitor the polar domains using a polarization microscope. Anisotropic crystals have an anisotropic dielectric susceptibility, ε, which is coupled to the refractive index (n). This anisotropic refractive index results in the decomposition of the incoming beam into one direct beam with polarization parallel to the anisotropy axis and one refracted beam with polarization perpendicular to the anisotropy axis. This phenomenon is known as birefringence.[32]

When a birefringent crystal with two orthogonal axes is placed between two polarizers, domains with varying orientations can be distinguished. In large Cu-hybrid crystals, areas with a different orientation of the easy axis (domains) could be observed (Figure 7).

The upper pictures were taken for the case where the polarizers P1 and P2 made an angle of 45°. In the lower pictures the polarizers were crossed at 90°. At low temperatures, various domains are clearly visible, which disappear in the high temperature phase. After cooling the sample back below T_c, only one domain remains. We note here that birefringence is not restricted to polar materials and is allowed for any orthorhombic crystal structure.

Although the pyroelectric current and capacitance measurements indicate hydrogen-bond based ferroelectric order in the Cu-hybrid, the X-ray diffraction data at 100 K were analyzed using the centrosymmetric space group *Pbca*. This space group does not allow and is inconsistent with the observation of ferroelectric order, thus the true symmetry is almost certainly lower. However, the breaking of inversion symmetry by a change in the hydrogen bonding pattern is not manifested in our diffraction data, as a consequence of the crystallographic "phase problem", where to a first approximation the intensities

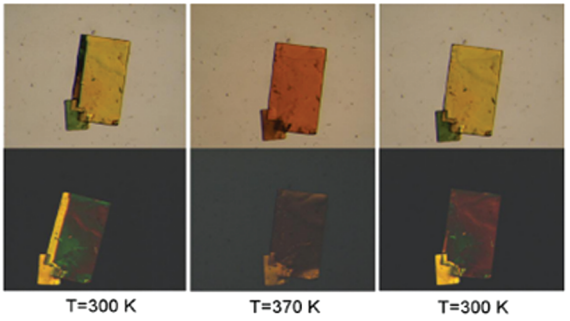

Figure 7. Birefringence in the Cu-based hybrid below and above the polar phase transition. The sample was placed between two polarizers that make an angle of 45° (upper images) and 90° (lower images). Left-hand images at 300 K: sample in the polar phase before heating. Middle images at 370 K: sample after heating through T_c. Right-hand images at 300 K: sample after cooling down to the initial state; the domains disappeared.

of Friedel reflection pairs $I_{(hkl)}$ and $I_{(-h-k-l)}$ are always equal. When anomalous dispersion corrections are included in the atomic scattering factors such that $f = f_0 + \Delta f' + i\Delta f''$, the imaginary term $\Delta f''$ can become significant and the intensities of Friedel pairs are unequal for polar structures. Nevertheless, such differences are typically difficult to measure experimentally, often being obscured by absorption corrections. In our case, the breaking of inversion symmetry involves light hydrogen and nitrogen atoms, with low scattering factors and large thermal motion that makes their contribution to the intensity at large scattering vectors small. Furthermore, in polar samples with near-equal populations of opposite ferroelectric domains, the difference between $I_{(hkl)}$ and $I_{(-h-k-l)}$ vanishes. Therefore, X-ray diffraction is often an unconvincing method to determine the presence or absence of inversion symmetry and is particularly problematic in the case of our Cu-hybrid. Although the space group *Pbca* that we use in our analysis forbids a macroscopic polarization, it does allow local dipole moments and is an accurate approximation of the structure based on electron density, capturing most of the structural degrees of freedom involved in the ferroelectric ordering, as discussed in detail below.

Further single crystal X-ray diffraction measurements at 370 K confirmed that the polar transition at 340 K is related to a change in crystal structure. The refined structural parameters obtained from the analysis of 1146 reflections are summarized in Table 1, and CIF files are included in the Supporting Information. At 370 K the structure was refined using the *Cmca* space group, in which the *c*-axis below T_c becomes the *a*-axis. In *Cmca* symmetry, the Cu, Cl, and various C atoms are located on special positions, in contrast to the case of *Pbca* where only Cu occupies a special position. Most of the interatomic distances increase with temperature, in line with the increase in lattice parameters. The only distance that significantly decreases above T_c is the Cu−Cl distance parallel to the *c*-axis, which exhibits a reduction of ~0.6%. The most striking difference between the high and the low temperature structures is the disappearance of the mirror plane that lies in the inorganic layer above T_c. This becomes a glide plane in the *Pbca* structure and allows buckling of the $CuCl_6$ octahedra to occur. In the paraelectric phase, the buckling of the octahedra completely disappears, as illustrated in Figure 8. We argue below that the origin of the electric polarization is a cooperative reorientation of the ammonium cations.[33]

dx.doi.org/10.1021/cm2023696 | *Chem. Mater.* 2012, 24, 133−139

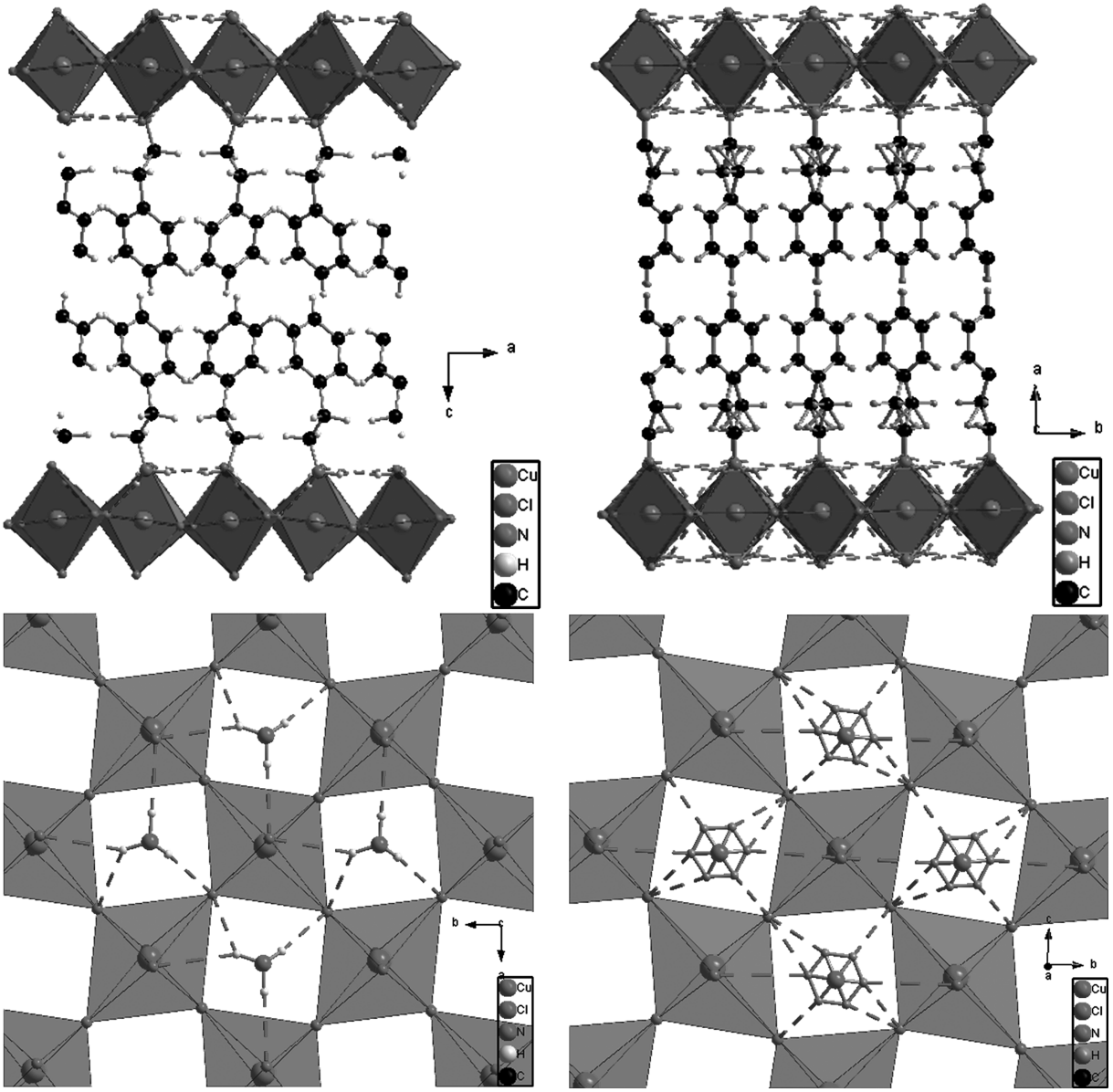

Figure 8. Top (lower) and side (upper) views of the crystal structure of $CuCl_4(C_6H_5CH_2CH_2NH_3)_2$ below (left) and above 340 K (right). In the high-temperature phase the buckling of the octahedra disappears. As a result, the hydrogen-bond network (dashed lines) changes.

DISCUSSION

We propose a hydrogen-bond ordering model to describe the transition at $T_c \sim 340$K, on the basis of our crystallographic data. In the nonpolar phase above T_c the ammonium groups can adopt several different but energetically equivalent orientations. An average of those positions is observed by diffraction and an ordered network of hydrogen bonds is absent. The (x, y) position of the nitrogen atom is located exactly in the middle of the square of coordinating metal cations.

The buckling of the octahedra below T_c results in a displacement of the ammonium groups and a cooperative hydrogen-bond ordering. Each ammonium then occupies a fixed position and the hydrogen bonds form an ordered network. This hydrogen-bond order is associated with a displacement of the nitrogen atom away from the middle of the square of metal cations that surround it. The displacement occurs in the direction of the hydrogen bond with the out-of-plane chlorine, thus in the opposite direction of the strongest hydrogen bond (Figure 9). This shift away from the strongest bonding chlorines is favorable, as it optimizes the hydrogen-bond (N−H−Cl) angles and the bond distances of both hydrogen bonds. The shift of the positively charged nitrogen atoms with respect to the negatively charged inorganic backbone generates a local dipole. In the *Pbca* space group, the displacements on both sides of the inorganic sheet are opposite and hence these local moments cancel. However, the pyroelectric current data provide evidence that the true symmetry is lower, allowing finite polarization.

The onset of the polar phase thus coincides with the buckling of the octahedra, which we assign as the primary order parameter of this phase transition. This buckling allows the ammonium groups to form static hydrogen bonds with one of the in-plane chlorine atoms and the out-of-plane chlorine atom, because both are displaced toward the nitrogen atom. The third hydrogen atom of the ammonium forms a weaker hydrogen bond, and in our model we neglect its role.

dx.doi.org/10.1021/cm2023696 | *Chem. Mater.* 2012, 24, 133−139

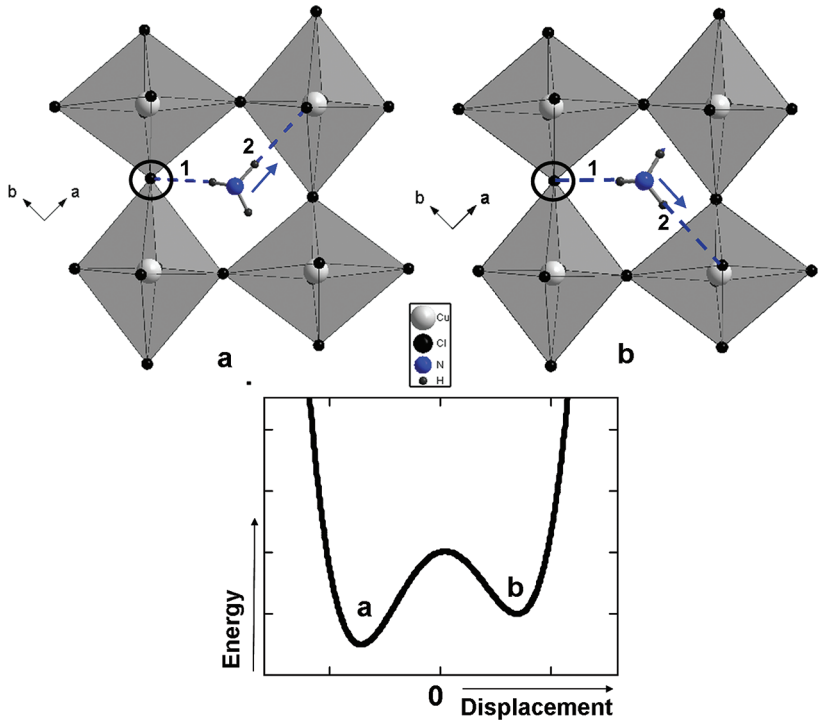

Figure 9. The ammonium group can occupy two different positions in the polar phase: (a) and (b). In both cases, the strongest hydrogen bond (1) is with the chlorine atom indicated by the circle. The second strongest hydrogen bond (2) is formed with an out-of-plane chlorine, which gives rise to the two options shown. Both situations lead to an off-center displacement of the nitrogen (denoted by the arrow). The atomic shifts generate a local electric dipole with both an in-plane and an out-of-plane component. Due to the buckling of the octahedra, both the magnitude and the direction of the dipole are different for (a) and (b). The energy landscape of the ammonium group can be represented by an asymmetric double potential well, as shown in the lower panel.

The first hydrogen bond is formed with an in-plane chlorine. From our X-ray diffraction data this bond exhibits the shortest bond length (2.321 Å) and a favorable N−H−Cl angle (172.28°). We therefore propose that this bond is the strongest—too strong to be influenced by the applied poling electric field. The second hydrogen bond is formed with an out-of-plane chlorine and is weaker due to the larger distance (2.368 Å) and less favorable angle (168.69°). There are two chlorine atoms available for this hydrogen bond. These chlorine atoms are crystallographically inequivalent as a result of the buckling of the inorganic sheet, and the resulting hydrogen bonds do not have the same energy. The ammonium group thus sees an asymmetric double potential well, as depicted in Figure 9. The two possible orientations of the second hydrogen bond, (a) and (b), give rise to different shifts of the nitrogen atom, the approximate directions of which are indicated by arrows in Figure 9. It should be noted that this shift also has an out-of-plane component, which is different for (a) and (b). As the nitrogen atom has a charge, the shift introduces a local dipole. If the material is not poled or strained, it is expected that all ammonium groups will adopt configuration (a), as this is lower in energy. This would result in an exact cancellation of all the local moments and no macroscopic polarization would be observed. However, when a poling field (E) is applied, the ammonium group can adopt configuration (b) and a net polarization can be generated. If the poling electric field is applied in the *ab* plane, some of the ammonium groups will favor situation (b), as its dipole has a component in the same direction as E. The ammonium groups on the other side of the inorganic slab would remain in configuration (a) as their dipoles do not have a component along E. The local displacement of nitrogen atoms introduces an internal electric field that tends to align the surrounding dipoles in the same direction. As a result of this cooperative distortion, the dipole moments do not exactly cancel, but give rise to a macroscopic polarization (P) along the direction of the poling field in the plane. For other directions of the electric poling field, this model will also result in a macroscopic polarization.

This model[34] is general and not restricted to the title compound. The key parameter for the generation of macroscopic polarization is the introduction of hydrogen-bond order by buckling of the perovskite-like sheet. The Jahn−Teller distortion present in the Cu-hybrid, where atomic displacements within the inorganic layer are caused by d-orbital degeneracy, does not seem to play any role in this mechanism. Our X-ray diffraction data indicate that the displacement of the ammonium group is ∼0.01 nm below T_c, which results in an in-plane polarization of a magnitude consistent with the pyroelectric current measurements. We note that a recent study of a similar $CuCl_4$-based hybrid, in which the organic part was ethyl ammonium instead of phenylethyl ammonium, reported multiferroic properties with a magnetic ordering temperature of 9 K and a spontaneous polarization of the order of 18 $\mu C/cm^2$.[35] The latter value is ∼1000 times larger than the polarization that we observe, and the large atomic displacements that are necessary to generate such a polarization are not consistent with our model.

In conclusion, the $CuCl_4(C_6H_5CH_2CH_2NH_3)_2$ hybrid with an inorganic perovskite-type structure is polar below T_c = 340 K, as evidenced by the observation of a macroscopic polarization below T_c. X-ray diffraction measurements show that this polarization is caused by a buckling of the perovskite

dx.doi.org/10.1021/cm2023696 | *Chem. Mater.* 2012, 24, 133−139

blocks that leads to ordering of the hydrogen bonds below T_c. This hydrogen-bond ordering results in a shift of the positively charged ammonium group with respect to the negatively charged inorganic backbone, generating a local dipole moment. Both capacitance measurements and the structural changes in the Cu-hybrid show a striking resemblance with the electrical properties of other improper ferroelectrics such as ARS.[11,30,36] Magnetic susceptibility measurements reveal ferromagnetic ordering below 13 K. Therefore, we provide evidence that this material exhibits a novel type of multiferroic behavior involving the coexistence of ferroelectricity originating from the organic block and ferromagnetism originating from the inorganic block. The electrical polarization and magnetic superexchange are both directly coupled to the buckling of the octahedra, and therefore, the magnetoelectric coupling induced by this mechanism is potentially very large.

■ ASSOCIATED CONTENT

Supporting Information

CIF files of $CuCl_4(C_6H_5CH_2CH_2NH_3)_2$ at 100 K and 370 K. This material is available free of charge via the Internet at http://pubs.acs.org.

■ AUTHOR INFORMATION

Corresponding Author

*E-mail: T.T.M.Palstra@rug.nl.

■ REFERENCES

(1) Eerenstein, W.; Mathur, N. D.; Scott, J. F. *Nature* **2006**, *442*, 759−765.
(2) Cheong, S.-W.; Mostovoy, M. *Nat. Mater.* **2007**, *6*, 13.
(3) Kimura, T. *Ann. Rev. Mat. Res.* **2007**, *37*, 387−413.
(4) van den Brink, J.; Khomskii, D. I. *J. Phys.: Condens. Mat.* **2008**, *20*, 434217.
(5) Kagawa, F.; Horiuchi, S.; Tokunaga, M.; Fujioka, J.; Tokura, Y. *Nature Phys.* **2010**, *6*, 169−172.
(6) Tokura, Y.; Seki, S. *Adv. Mater.* **2010**, *22*, 1554−1565.
(7) Wu, S. M; Cybart, S. A.; Yu, P.; Rossell, M. D.; Zhang, J. X.; Ramesh, R.; Dynes, R. C. *Nat. Mater.* **2010**, *9*, 756−761.
(8) Ohkoshi, S; Tokoro, H.; Matsuda, T.; Takahashi, H.; Irie, H.; Hashimoto, K. *Angew. Chem., Int. Ed.* **2007**, *46*, 3228−3241.
(9) Mitzi, D. B. *Prog. Inorg. Chem.* **1999**, *48*, 1−121.
(10) Horiuchi, S.; Tokura, Y. *Nat. Mater.* **2008**, *7*, 357−366.
(11) Ishibashi, Y.; Takagi, Y. *Jpn. J. Appl. Phys.* **1976**, *15*, 1621−1636.
(12) Hoshino, S.; Okaya, Y.; Pepinsky, R. *Phys. Rev.* **1959**, *115*, 323−330.
(13) Jain, P.; Ramachandran, V.; Clark, R. J.; Zhou, H. D.; Toby, B. H.; Dalal, N. S.; Kroto, H. W.; Cheetham, A. K. *J. Am. Chem. Soc.* **2009**, *131*, 13625−13627.
(14) Ramesh, R. *Nature* **2009**, *46*, 1218−1219.
(15) Arkenbout, A. H.; Uemura, T.; Takeya, J.; Palstra, T. T. M. *Appl. Phys. Lett.* **2009**, *95*, 173104.
(16) *SMART*, version 5.632; Bruker AXS Inc.: Madison, WI; *SAINT-Plus*, version 6.45; Bruker AXS Inc.: Madison, WI.
(17) Beurskens, P. T.; Beurskens, G.; de Gelder, R.; Smits, J. M. M.; García-Granda, S.; Gould, R. O. *DIRDIF-08*, Program System; Crystallography Laboratory, University of Nijmegen: The Netherlands, 2008.
(18) Sheldrick, G. M. *SHELXL97*, Program for Crystal Structure Refinement; University of Göttingen: Germany, 1997.
(19) Willett, R. D. *Acta Crystallogr.* **1990**, *C46*, 565−568.
(20) Willett, R.; Place, H.; Middleton, M. *J. Am. Chem. Soc.* **1988**, *110*, 8639−8650.
(21) Rubenacker, G.; Haines, D. N.; Drumheller, J. E.; Emerson, K. *J. Magn. Magn. Mater.* **1984**, *43*, 238−242.
(22) Long, G. S.; Wei, M.; Willet, R. D. *Inorg. Chem.* **1997**, *36*, 3102−3107.
(23) Khomskii, D. I.; Kugel, K. I. *Solid State Commun.* **1973**, *13*, 763−766.
(24) Estes, W. E.; Losee, D. B.; Hatfield, W. E. *J. Chem. Phys.* **1980**, *72*, 630−638.
(25) de Jongh, L. J.; van Amstel, W. D.; Miedema, A. R. *Physica B* **1972**, *58*, 277−304.
(26) Yurtseven, H.; Sherman, W. F. *J. Mol. Struct.* **1984**, *115*, 169−172.
(27) van Roie, B.; Leys, J.; Denolf, K.; Glorieux, C.; Pitsi, G.; Thoen, J. *Phys. Rev. E* **2005**, *72*, 041702.
(28) Dultz, W. *Solid State Commun.* **1974**, *15*, 595−598.
(29) Caretta, A. Paper in preparation.
(30) Mitsui, T.; Furuichi, J. *Phys. Rev.* **1953**, *90*, 193−202.
(31) Cohen, R. E. *Nature* **1992**, *358*, 136−138.
(32) Wemple, S. H.; Didomenico, M.; Camlibel, I. *J. Phys. Chem. Solids* **1968**, *29*, 1797−1803.
(33) Brozek, Z.; Mucha, D.; Stadnicka, K. *Acta Crystallogr.* **1994**, *B50*, 465−472.
(34) Arkenbout, A. H. PhD thesis series, Zernike Institute 2010.
(35) Kundys, B.; Lappas, A.; Viret, M; Kapustianyk, V.; Rudyk, V.; Semak, S.; Simon, Ch.; Bakaimi, I. *Phys. Rev. B* **2010**, *81*, 224434.
(36) Sawada, A.; Takagi, Y. *J. Phys. Soc. Jpn.* **1972**, *33*, 1071−1075.